ChemPubSoc Europe

DOI: 10.1002/cplu.201900528

CHEMPLUSCHEM Full Papers

Crosslinkable Bis(diphenylamine)-Substituted Mixed Dihydroindeno[1,2-*b*]fluorenes for Solution-Processed Multilayer Organic Light-Emitting Diodes

Matthias Hempe,[a] Johanna Paschek,[b] Jürgen Schelter,[b] Anne Umbach,[c] Klaus Meerholz,*[b, c] and Michael Reggelin*[a]

The synthesis and application of a series of crosslinkable bis(diphenylamine)-substituted mixed dihydroindeno[1,2-*b*]fluorenes as model systems for the fabrication of solution-processed, multilayer organic light-emitting diodes (OLEDs) is described. Introducing a novel functionalization approach by $C(sp^3)$–$C(sp^2)$ Suzuki-Miyaura reactions, the synthesis is based on a modular strategy, leading to eight nearly isoelectronic derivatives that allow for the observation of structure-property relationships in the context of crosslinkable hole-transport materials, e.g., for use in OLEDs. By systematically altering structural parameters, such as the number of crosslinkable oxetane moieties per molecule (2–6 moieties) and their position of attachment (geminal and/or lateral), process-relevant thermal properties such as thermal stability (T_d95, 170-350°C) and glass-transition temperature (15-100°C) can be influenced and allow for the investigation of their impact on the crosslinking behavior and the resulting device performance.

1. Introduction

In current commercial applications, small molecule organic semiconducting materials are most commonly processed by vacuum deposition techniques to fabricate state-of-the-art, high performance multilayer OLED devices. To realize future large-area OLEDs, processing of the functional materials by low cost, high-throughput, solution-based methods is favorable. Unfortunately, commonly used small molecules often possess insufficient solubilities, and suffer from poor film forming properties and/or poor solvent orthogonality. This leads to intermixing or dissolution phenomena upon the processing of subsequent layers and results in poor device performances. To cast defined multilayer architectures from solution, two main issues must be considered:

1) The formation of homogenous films: It has been shown that besides their intrinsic electronic properties, the morphology and thin film stability of the organic molecules is of vital importance for the effectiveness and durability of the resulting devices.[1] The amorphous, glassy arrangement of the molecules within each layer has been identified as beneficial for OLED devices.[2] To cast homogenous films from solution, the glass-transition temperature (T_g) of the materials is a highly relevant parameter. In this context, low-T_g materials favor the formation of smooth films, while high-T_g materials are necessary for durable device performance.[3]

2) The preservation of film integrity upon the deposition of subsequent layers: One strategy to achieve this is the polymerization of crosslinkable moieties. In this respect, the use of oxetanes, which can be crosslinked through cationic ring-opening polymerization reactions (CROP),[4] has been demonstrated in the field of hole-transporting[5] and light-emitting materials.[6] The attachment of oxetane units through spacing alkyl chains can lead to materials with high solubility, good film forming properties, and low volume shrinkage upon polymerization, which is a prerequisite for the fabrication of high-performance OLED devices.[7] Additionally, it was shown that the polymerization of oxetanes can even be used to preserve ordered molecular arrangements within the solid state.[8] In the course of the polymerization reaction, the vitrification of the layer reduces the molecular mobility and increases the glass transition temperature of the film. Thereby, the mechanical properties of the resulting network depend on the mesh size and the number of nodal points. Thus, even high-T_g morphologies for durable device performance can be achieved by post-deposition polymerization of low-T_g oxetane-functionalized materials.

[a] *Dr. M. Hempe, Prof. M. Reggelin*
Clemens-Schöpf-Institut für Organische Chemie und Biochemie
Technische Universität Darmstadt
Alarich-Weiss-Straße 4
64287 Darmstadt (Germany)
E-mail: re@chemie.tu-darmstadt.de
[b] *Dr. J. Paschek, Dr. J. Schelter, Prof. K. Meerholz*
Institut für Physikalische Chemie
Universität zu Köln
Luxemburger Str. 116
50939 Cologne (Germany)
E-mail: klaus.meerholz@uni-koeln.de
[c] *Dr. A. Umbach, Prof. K. Meerholz*
née Köhnen
ZOEK gGmbH
COPT-Zentrum der Universität zu Köln
Luxemburger Str. 90
50939 Cologne (Germany)

Supporting information for this article is available on the WWW under https://doi.org/10.1002/cplu.201900528

To hamper crystallization of the molecules before crosslinking and, therefore, ensure their amorphous arrangement, several molecular design strategies have been developed, one of which is the introduction of sterically demanding spiro units to the molecular backbone of fluorene and dihydroindeno[1,2-*b*]fluorene derivatives.[9] Here, especially aryl substituents have been successfully used to prevent molecular aggregation by steric hindrance.[10] Additionally, it has been shown that by the attachment of arylamines to dihydroindeno[1,2-*b*]fluorene scaffolds, high performance hole transport materials (HTM) can be obtained.[11]

In this paper, we report on the syntheses and application of crosslinkable bis(diphenylamine)-substituted dihydroindeno-[1,2-*b*]fluorenes as HTM for solution-processed multilayer OLED devices (Figure 1). Here, the mixed substituted dihydroindeno-[1,2-*b*]fluorene (MIF)[12] core structure was used to combine morphological stability by spiro-aryl substituents with an easy to functionalize central, benzylic position for alkyl-substituent attachment.[13] The system allows for the variation of the number of crosslinkable units per molecule (2-6 oxetanes), as well as a variation in the positions of attachment (geminal and/or lateral) of these moieties onto the rigid, high-T_g molecular backbone. The attachment of the alkyl-bound oxetane moieties in the lateral positions of the molecules was realized through a novel synthetic approach, involving the C(sp^3)-C(sp^2) cross-coupling reactions of oxetane-substituted potassium trifluoroborates with halogenated diphenylamine intermediates. This strategy enables the synthesis of nearly isoelectronic derivatives by a modular approach. Thus, a set of materials is obtained which permits the investigation of the influence of the above structural modifications on process-relevant properties such as thermal stability, glass transition temperature, crosslinking behavior, and its impact on the resulting device performance. The performance of the novel materials is compared with commonly used oxetane-functionalized, benzidine-type hole conductors based on the TPD motif (triphenylamine dimer) as well as fully alkyl-substituted dihydroindeno[1,2-*b*]fluorenes.

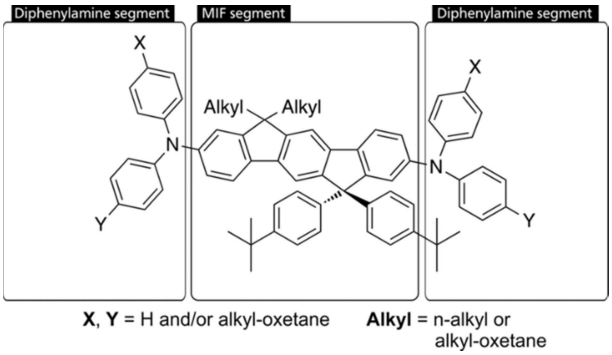

Figure 1. Target structures of the DPA-MIF series reported in this work.

2. Results and Discussion

2.1. Synthesis

The synthesis of the materials is based on a modular approach involving Buchwald-Hartwig amination reactions of the mixed dihydroindeno[1,2-*b*]fluorene (MIF) core structures and diphenylamine (DPA) components at the final stage. Here, the syntheses of the DPA components **5a–b** involve a novel, selective functionalization strategy through C(sp^3)-C(sp^2) cross-coupling of an oxetane-substituted potassium trifluoroborate **3** and diarylamine halides **4a–b**. By permutation of oxetane-functionalized and unfunctionalized diphenylamine- and MIF-components, a series of eight nearly isoelectronic derivatives **9** was obtained.

Starting from the oxetane alcohol **1**, the syntheses of haloalkane-substituted oxetanes **2a–c** of varying alkyl chain length were achieved by etherification (Scheme 1).[5b] Thereafter, compound **2** was converted to the oxetane-substituted potassium trifluoroborate **3**, which was successfully cross-coupled with the halogenated diphenylamines **4a** and **4b** to obtain the mono- and bis-oxetane functionalized diphenylamine components **5a–b**. It is important to note that the oxetane-substituted potassium trifluoroborate **3** is a novel, highly versatile building block for the general synthesis of crosslinkable aromatic materials. Similar to the primary alkyl trifluoroborates reported by Molander *et al.*,[14] compound **3** can be stored under ambient conditions for months, with no special precautions. Moreover, the cross-coupling reactions in this work even proceed in the presence of the free N–H functionality of the secondary amines **4a–b** and do not require additional protecting group chemistry of their acidic molecular positions. Therefore, this functionalization strategy represents an interesting alternative to traditional synthetic approaches, commonly

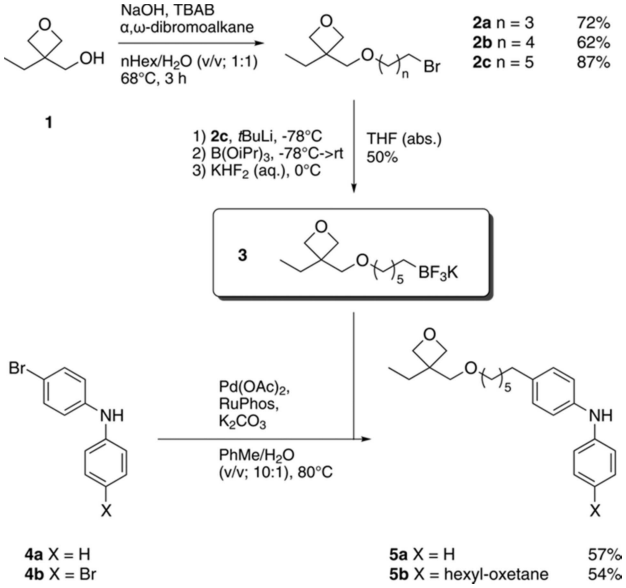

Scheme 1. Reaction sequence to diphenylamines **5a** and **5b** involving key Suzuki-Miyaura cross-coupling reaction of oxetane-functionalized potassium trifluoroborate **3** and halogenated diphenylamines **4a–b**.

involving a sequence of lithiation and nucleophilic substitution reactions, which are not compatible with this kind of substrates.[15]

The syntheses of the MIF compounds **8a–d** are in principle based on the synthetic strategies of symmetrically substituted dihydroindeno[1,2-*b*]fluorenes.[10a,d,16] However, due to the susceptibility of the oxetane moieties towards electrophiles and with respect to the derivatization approach, the attachment of the alkyl substituents to the MIF core reported in this work was accomplished in the last stage of the MIF dibromide **8** synthetic sequence (Scheme 2). As reported previously, the synthesis of the respective MIF starting material **6** was realized in two isolated reaction steps.[13] The copper(II) bromide mediated bromination[17] of the MIF structure **6** was followed by the alkylation of the benzylic 12,12′-positions of **7** with various haloalkane electrophiles (1-bromobutane or **2a–c**), which finally yielded the key MIF intermediates **8a–d**.

The Buchwald-Hartwig amination reactions of the dibromides **8a–d** with diphenylamine led to the unfunctionalized reference compound REF **9a**, as well as to the geminally functionalized derivatives **9b–9d**. The twofold laterally functionalized material 2L6-0G **9e**, and the fourfold oxetane-substituted compound 2L6-2G6 **9f** were obtained by the coupling reactions of **8a** and **8d** with the mono-functionalized diphenylamine **5a**. The syntheses of the fourfold laterally functionalized compound 4L6-0G **9g** and the sixfold oxetane-substituted molecule 4L6-2G6 **9h** were achieved by the reaction of **8a** and **8d** with the bis-oxetane-substituted diphenylamine component **5b**. Throughout the remainder of the paper we will refer to the different DPA-MIFs as xLm-yGn, where "x" and "y" indicate the number of oxetane groups for the lateral ("L") and geminal ("G") positions, while "m" and "n" indicate the length of the alkyl spacer between the molecular core and the oxetane group for "L" and "G" positions.

2.2. Solid-State Structure of REF 9a

The solid-state structure of the unfunctionalized DPA-MIF **9a** was elucidated by single crystal x-ray analysis. The compound was recrystallized from ethyl acetate, yielding the space group P-1 (triclinic, Figure 2). In every unit cell, two molecules are in coplanar arrangement while being shifted relative to one another. The lateral diphenylamine substituents are slightly bent out of plane, distorting the aromatic dihydroindeno[1,2-*b*]-fluorene backbone. Within the molecular packing, no cofacial arrangement of the dihydroindenofluorene structures was observed. While the dihydroindenofluorene core structures are spatially well separated and do not overlap, the closest intermolecular C–C-distance between two arylamine units of one layer was determined to be 3.737 Å. Between the layers, the shortest contact of arylamines has been determined to be

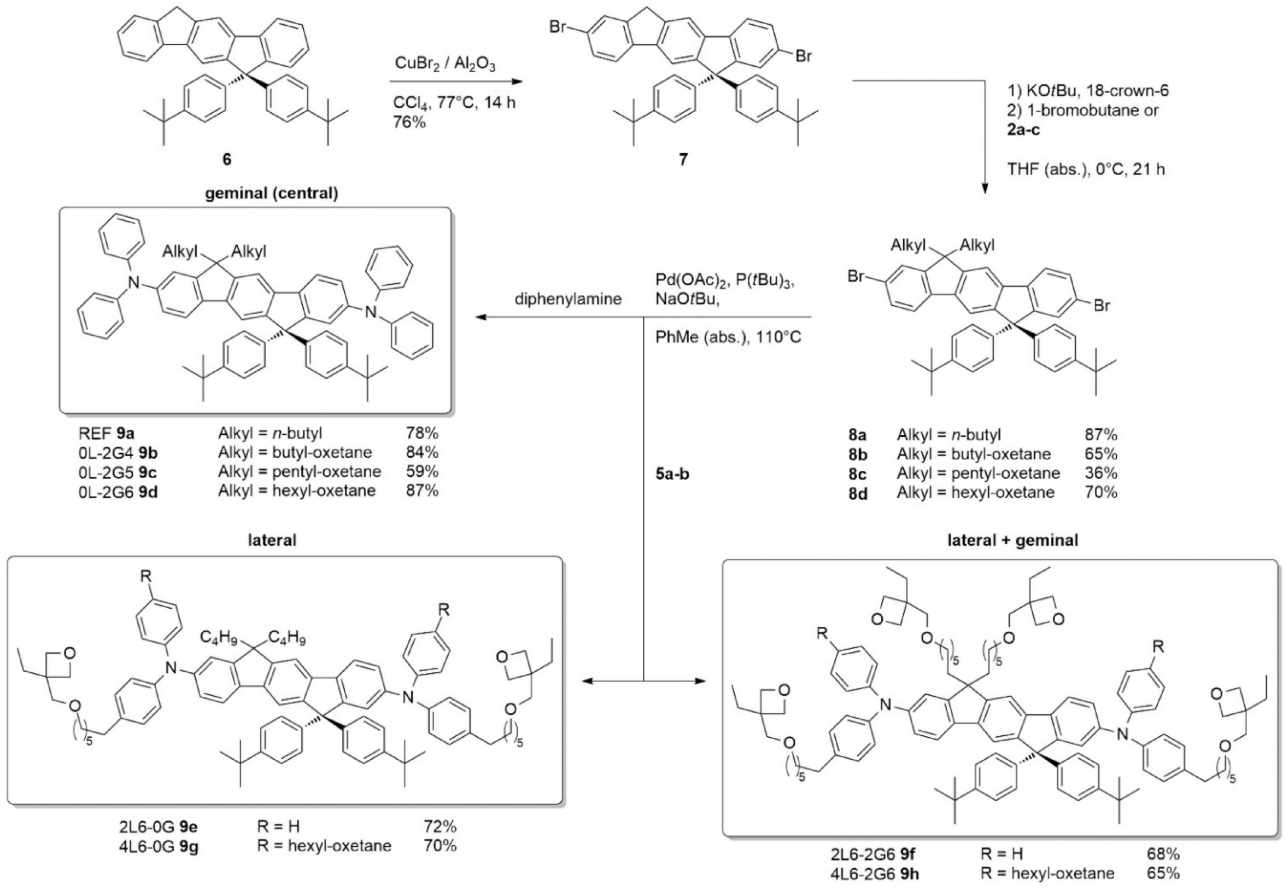

Scheme 2. Synthesis of DPA-MIF derivatives **9a–h**.

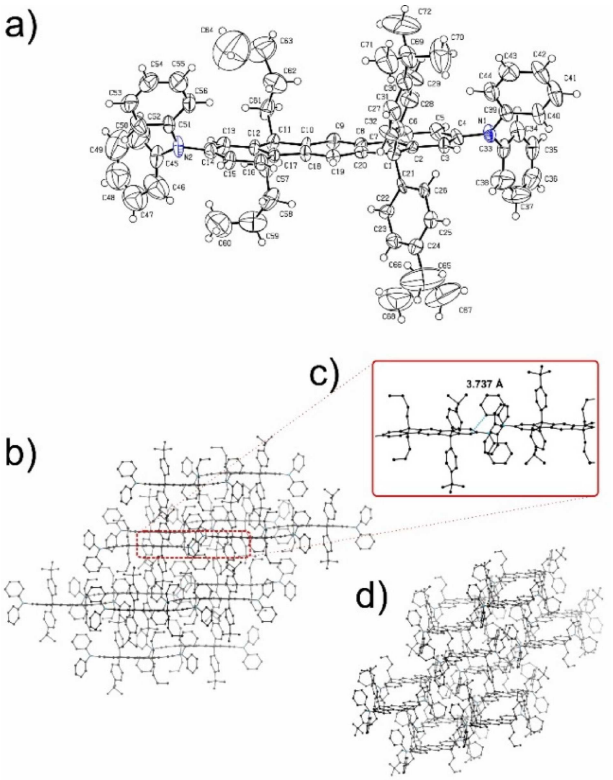

Figure 2. a) ORTEP plot of the molecular structure of 12,12′-dibutyl-6,6′-di(4-*tert.*-butylbenzene)-N^4,$N^{4'}$,N^{10},$N^{10'}$-tetraphenyldihydroindeno[1,2-*b*]fluorene-4,10-diamine (REF **9a**). b) coplanar molecular packing, c) detailed view of the closest intermolecular contact, d) side view of coplanar molecular packing (H atoms have been omitted for clarity).

4.577 Å. These short intermolecular distances can be beneficial for hole transportation. All other compounds **9b**–**h** do not crystallize due to the decoration with the alkyl-bound oxetane units.

2.3. Thermal Properties

The thermal properties of the DPA-MIF materials were investigated by thermal gravimetric analysis (TGA) and differential scanning calorimetry (DSC, Table 1 and SI). To evaluate the thermal stability of the derivatives, the decomposition temperature T_d^{95} was determined. Due to the different molecular weights of the derivatives investigated, this parameter should only be used for qualitative evaluation (for detailed TGA analyses, see Supporting Information). The TGA analyses reveal an intrinsic instability of the geminal *n*-butyl substituents (**9a**, **9e** and **9g**) at temperatures higher than 100 °C. In contrast to this, longer alkyl-oxetane substituents in the geminal positions lead to materials of higher thermal stability (**9b**–**d**, **9f**, **9h**). The geminally functionalized materials **9b**–**d** show high thermal stabilities with T_d^{95} parameters higher than 350 °C. This tendency can also be observed comparing the thermal stability of the fourfold functionalized compounds 2L6-2G6 **9f** (T_d^{95} 270 °C) and 4L6-0G **9g** (T_d^{95} 220 °C).

Table 1. Thermal properties of the DPA-MIF derivatives **9a**–**h**.

	T_d^{95} [°C][a]	T_g [°C][b]
REF **9a**	153	not observed[c]
0L-2G4 **9b**	355	100
0L-2G5 **9c**	>350	83
0L-2G6 **9d**	350	69
2L6-0G **9e**	170	38
2L6-2G6 **9f**	270	36
4L6-0G **9g**	220	18
4L6-2G6 **9h**	250	15

[a] T_d^{95}: decomposition temperature determined by TGA (temperature at 5% weight loss, N_2 atmosphere, 10 K/min), [b] T_g: glass transition temperature determined by DSC in second heating cycle (N_2 atmosphere, 10 K/min), [c] Temperature range between 0 °C and 110 °C.

For the processing of the materials from solution, the glass transition temperature (T_g) is of high importance. Here, the DPA-MIF derivatives follow a clear trend. In case of the geminally functionalized materials **9b**–**d**, a lowering T_g from 100 °C to 69 °C can be observed when increasing the length of the spacing alkyl chains from butyl to hexyl. By laterally attaching two hexyl-bound moieties to the molecular structure, T_g can be significantly lowered to 38 °C (2L6-0G **9e**). Here, the attachment of further alkyl-oxetane substituents in the central, geminal position has only minor impact on T_g (2L6-2G6 **9f**, T_g 36 °C). In case of the fourfold laterally functionalized derivatives **9g**–**h**, the glass transition temperature is lowered even further (18 °C and 15 °C), however, the impact of increasing number of oxetane units is surprisingly small. By comparing the T_g of DPA-MIF derivatives with identical number of oxetane units, but which differ in their position of functionalization, it becomes obvious that the lateral attachment reduces T_g more strongly than the geminal attachment. Comparing the glass transition temperatures of the DPA-MIF materials to the twofold oxetane-functionalized materials OTPD and QUPD (T_g −5 °C and −1 °C) reported in the literature,[5c] it can be seen that the rigid dihydroindeno[1,2-*b*]fluorene backbone bearing two aryl substituents generally leads to higher T_g materials than the benzidine-based molecules.

2.4. Electronic and Optical Characterization

The electronic and optical properties of the series of materials have been investigated by cyclic voltammetry (CV), UV/vis, and photoluminescence (PL) spectroscopy, respectively (see Table 2). Due to the identical electronic situation of **9a** and the geminally functionalized derivatives **9b**–**d**, the latter have been omitted from this investigation. The minor electronic impact of the number of laterally attached alkyl-oxetane substituents was observed by optical spectroscopy (Figure 3). Here, the two- and fourfold functionalized compounds 2L6-0G **9e** and 4L6-0G **9g** have been studied as examples and have been compared to the unfunctionalized compound DPA-MIF REF **9a**.

The DPA-MIF-reference REF **9a** features two chemically reversible oxidation steps with half-wave potentials at $E_{Ox,1}$ (+0.23 V) and $E_{Ox,2}$ (+0.44 V) vs. ferrocene/ferrocenium ($FeCp_2$/$FeCp_2^+$) (the cyclic voltammogram is given in the Supporting

Table 2. Optical and electronic properties of the derivatives REF **9a**, 2L6-0G **9e**, 4L6-0G **9g** in comparison to the dihydroindeno[1,2-*b*]fluorene 3Ph by Wong *et al.*,[16b] the benzidine-based materials QUPD and OTPD, as well as the dihydroindenofluorene-based material JS247 (structures given in the Supporting Information).

	$E^{1/2}_{Ox1}$ [a] [V vs. Fc/Fc^+]	λ_{abs} [nm][b]	λ_{PL} [nm][b]	ΔE_{opt} [eV][c]	HOMO [eV][d]	LUMO [eV][e]
3Ph[16b]	1.44	347	353	3.53	−6.40	−2.87
REF **9a**	0.23	402	417	2.98	−5.33	−2.35
2L6-0G **9d**	0.20[f]	405	421	2.95	−5.30	−2.35
4L6-0G **9g**	0.18[f]	408	424	2.93	−5.28	−2.35
QUPD	0.07	353	423	3.12	−5.17	−2.05
OTPD	0.24	354	404	3.17	−5.34	−2.17
JS247	0.11	404	423	2.93	−5.21	−2.28

[a] Obtained in DCM/$TBAPF_6$, T = 298 K, 20 mV/s. [b] At maximum intensity, respectively, excited at λ_{abs}. [c] From absorption edge of UV/vis spectra. [d] Calculated from the first oxidation potential using $E_{HOMO} = -5.1 - E^{1/2}_{Ox,1}$.[5c] [e] Determined by the optical bandgap and HOMO energy. [f] Estimated considering additional alkyl substituents.

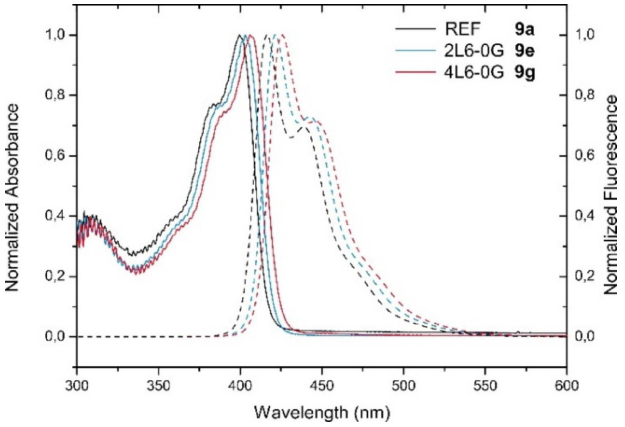

Figure 3. Absorption spectra (bold lines) and photoluminescence spectra (dashed lines) of REF **9a**, 2L6-0G **9e** and 4L6-0G **9g** in THF (excited at λ_{abs}).

Information). Due to the isoelectronic nature of the compounds **9b**–**9d**, very similar values can be assumed.

By introducing more and more alkyl substituents in the peripheral positions (compounds **9e** and **9f** have 2 additional alkyl substituents; compounds **9g** and **9h** have 4 additional alkyl substituents), a lower oxidation potential is expected. Comparison with the basic molecular structure of 3Ph reported by Wong *et al.*[16b] (the molecular structure is given in the Supporting Information) shows, that both oxidation potentials are shifted towards more positive values, which can be attributed to the electron-rich nature of the diphenylamine substituents and the extension of the conjugated π-electron system. Further, compared to a dihydroindenofluorene featuring all-alkyl-substitution at the core (compound JS247, Supporting Information), which is oxidized at 0.11 V vs. ferrocene under identical conditions, the higher oxidation potential of **9g** (and the isoelectronic **9h**) might be indicative of stronger twisting of the MIF core compared to dihydroindenofluorene.

To estimate the HOMO energy level of the DPA-MIF compounds, the first oxidation potential was used in accordance to an established procedure: $E_{HOMO} = -5.1 - E_{ox}$.[5c] Here, the HOMO energy level of the diphenylamine-substituted compound REF **9a** was determined to −5.33 eV. Thus, the DPA-MIF materials are easily oxidized and should allow for efficient hole transportation. The energy level of the LUMO could not be obtained directly by electrochemical analysis, since the electrochemical window is too small. Therefore, the energy of the optical bandgap was derived from the absorption edge of the of UV/vis spectrum and was used to calculate the LUMO energy of DPA-MIF **9a** (−2.35 eV) (Table 2). This energy level was found to be sufficiently high to efficiently block electrons from adjacent layers of an OLED device, resulting in good charge confinement within the emissive layer.

The absorption spectrum of compound **9a** presents an absorption maximum at 402 nm and hence is bathochromically shifted with respect to 3Ph (347 nm). Similar to the ladder-type oligophenylene arylamines reported by Fan *et al.*,[18] the spectrum features two prominent bands, which were assigned to the n→π* transition of the triarylamine moieties and π→π* transition of the dihydroindenofluorene core. The mirror-image like photoluminescence spectrum of DPA-MIF **9a** exhibits a small Stokes shift of 15 nm and presents an emission maximum at 417 nm (3Ph, 353 nm). To investigate the electronic impact of the number of laterally attached alkyl-oxetane substituents, compounds 2L6-0G **9e** and 4L6-0G **9g** have also been characterized by optical spectroscopy. Along the series of REF **9a**, 2L6-0G **9e** and 4L6-0G **9g**, the absorption edge of the spectra bathochromically shifts by 3 nm (23 meV) for each compound, respectively. This small bathochromic shift can be observed in the emission spectra as well, demonstrating the low electronic impact of the novel functionalization strategy by $C(sp^3)$-$C(sp^2)$ cross-coupling reactions. Hence, the DPA-MIF series presented here is in principle well suited for a comparative study of their respective OLED performance.

2.5. Crosslinking Behavior

The impact of the structural modifications on the crosslinking behavior of the DPA-MIF derivatives was investigated by photoacid-initiated crosslinking experiments under inert atmosphere using the photoacid generator (PAG) 4-octyloxydiphenyliodonium hexafluoroantimonate(V) (OPPI) reported by Crivello *et al.* (Table 3).[19] After the deposition of the functional ink onto the glass substrate, the PAG was activated by UV irradiation at 365 nm. Thereafter, it was necessary to promote the crosslinking reaction by thermal curing of the film. Due to gelation and vitrification, the curing temperature should in general be higher than the glass transition temperature T_g of the respective material in order to propagate network formation.[20] Here, the diffusional mobility of the functional moieties can be inversely correlated to T_g, which rapidly increases in the course of the polymerization reaction. Consequently, the ideal crosslinking temperature should be set in agreement with the efficient formation of the macromolecular network and in respect to the thermal stability of the materials. The topography of crosslinked films has been investigated by atomic force microscopy (AFM).

Table 3. Crosslinking of DPA-MIF derivatives **9d**–**h** spin-coated from toluene solution onto glass substrates (N_2 atmosphere).

No.		T_g [°C]	OPPI [mol %][a]	curing	SR [%][b]
1	0L-2G6 **9d**	69	2	5 min, 130 °C	0
2			2	5 min, 150 °C	16
3			4 (OLED)[c]	5 min, 150 °C	100
4	2L6-0G **9e**	38	2	5 min, 100 °C	0
5			2	5 min, 130 °C	0
6			4	5 min, 150 °C	0
7	2L6-2G6 **9f**	36	2	5 min, 130 °C	79
8			3	5 min, 130 °C	77
9			4	5 min, 130 °C	88
10	4L6-0G **9g**	18	2	5 min, 130 °C	93
11			3	5 min, 130 °C	100
12	4L6-2G6 **9h**	15	2 (OLED)[c]	5 min, 150 °C	100

[a] 4-Octyloxydiphenyliodonium hexafluoroantimonate(V) (OPPI) used as photoacid generator. [b] Solvent resistivity (SR) determined by profilometry analysis of film thickness before and after rinsing of the photopolymerized film. [c] Indicating the conditions used for OLED device fabrication.

The average RMS roughness is typically below 1 nm. Non-crosslinked films cannot be investigated, because they are very soft. It is assumed that the topography is similar to the one after crosslinking.

Owing to their rather elevated T_g (Table 1), the derivatives 0L-2G4 **9b** and 0L-2G5 **9c** have not been investigated here. In the case of 0L-2G6 **9d** and 2L6-0G **9e**, crosslinking of films of the two derivatives using 2 mol% of the PAG at 130 °C does not lead to the formation of solvent-resistant, macromolecular networks (entries #1 and #5). While increasing the curing temperature to 150 °C does not enhance the resulting solvent-resistivity significantly (entry #2), the additional increase of the amount of the PAG results in fully insoluble films of the derivative 0 L-2G6 **9d** (entry #3). In contrast to this, the crosslinking of the laterally functionalized material 2 L6-0G **9e** under these conditions does not lead to solvent-resistant films despite the lower T_g (entry #6). The reason for this unexpected behavior is unknown at this point.

In the case of the fourfold functionalized materials 2L6-2G6 **9f** and 4L6-0G **9g** it can be seen that under identical crosslinking conditions, the lower-T_g material **9g** can be used to obtain films of higher solvent resistivity due to better network formation (entries #7 and #10, as well as #8 and #11).

Another structural parameter of high importance is the number of crosslinkable moieties per molecule. Along the series of experiments, less of the initiating PAG was necessary for the derivatives of higher numbers of oxetane groups per molecule. This can be explained by the higher density of reactive sites within the film resulting in a higher probability for crosslinking in the course of the living chain-growth polymerization reaction. Thus, less points of initiation are necessary for the formation of the extended macromolecular network, already leading to insoluble films of the sixfold functionalized material 4L6-2G6 **9h** when using only 2 mol % of the PAG (entry #12).

2.6. OLED Performance

To evaluate the potential of the synthesized DPA-MIF derivatives in organic electronic devices, two materials, 0L-2G6 **9d** and 4L6-2G6 **9h**, were applied as hole-transport materials (HTM) in solution-processed, multilayer OLEDs. The selection of these two materials was based on their good thermal stability and crosslinking behavior. Additionally, the application of these two materials should demonstrate the impact of the number of oxetane functions on the OLED performance, going from two (0L-2G6 **9d**) to six (4L6-2G6 **9h**) crosslinkable moieties per molecule, and thus enhancing the possible number of nodal points within the layer.

Within the series of OLED devices, a standardized stack architecture ITO/PEDOT (44 nm)/xHTM (30 nm)/F8BT (80 nm)/CsF (3.5 nm)/Al (100 nm) was used to compare the OLED performance of the DPA-MIF derivatives versus the performance of established, benzidine-based materials (Figure 4, Table 4). Here, the twofold functionalized, crosslinkable hole-transport materials QUPD and OTPD were used (molecular structures are given in the Supporting Information).[5c] For crosslinking of the oxetane-functionalized materials, the lowest amount of the PAG was used, which still led to the formation of completely insoluble films. To prevent doping by radical cations generated during the crosslinking process,[21] the hole-transport layers were treated thermally in a post-processing step at elevated temperatures (110 °C for 2 minutes) prior to the deposition of the emitting material F8BT from solution (for details on crosslinking conditions and solution-processing see Supporting Information). The morphology of the EML does not show any features just like the HTL, the surface roughness is below 1 nm RMS, i.e., similar to the underlying HTL, thus, there is - as expected - no impact of the HTL on the EML.

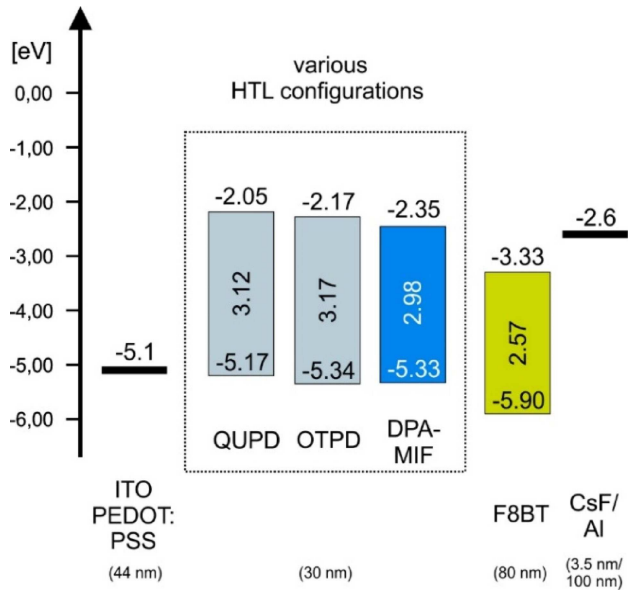

Figure 4. Energy level diagram of the OLED device configurations investigated within the series.

Table 4. Summary of the device performances of solution-processed, standardized OLED stacks using various xHTL configurations (ITO/PEDOT:PSS/xHTL/F8BT/CsF/Al). The devices are ordered regarding the HOMO level of the xHTM, respectively.

xHTL	# oxetanes[a]	OPPI [mol%]	E_{HOMO} [eV]	E_{LUMO} [eV]	U_{on} [V][b]	L [cd/m^2][c]	LE [cd/A] @ 100 cd/m^2	LE [cd/A] @1000 cd/m^2
QUPD (30 nm)	2	1	−5.17	−2.05	2.3	2,000	0.30 (4.41 V)	0.38 (7.59 V)
4L6-2G6 **9h** (30 nm)	6	2	−5.28	−2.35	2.9	300	0.35 (7.31 V)	–
0L-2G6 **9d** (30 nm)	2	4	−5.33	−2.35	2.9	5,000	1.49 (4.89 V)	1.81 (6.84 V)
OTPD (30 nm)	2	0.5	−5.34	−2.17	2.5	1,250	1.12 (5.42 V)	1.11 (8.60 V)

[a] Number of oxetane units per molecules. [b] U [V] @1 cd/cm^2. [c] @9 V.

All devices showed bright green-yellow electroluminescence, featuring a peak at ca. 575 nm (see Figure S4 in the Supporting Information). The turn-on voltage increases in the sequence QUPD < OTPD < **9d** = **9h**. The fact that both MIF-compounds feature a higher turn-on voltage despite their more favorable E(HOMO) might be attributed to a reduced hole mobility as compared to the TPD-derivatives. Among the devices, the one based on **9d** features the lowest operating voltage for an EL of 1000 cd/m^2 (6.8 V) as well the highest current efficiency (1.8 cd/A) obtained at a brightness of 1000 cd/m^2, both indicative of a more favorable hole/electron balance, resulting in improved recombination and, thus, emission.

3. Conclusion

In summary, a highly modular synthetic route to a series of oxetane-functionalized, bis(diphenylamine)-substituted mixed dihydroindenofluorenes (DPA-MIFs) is presented. The reaction sequence involves a novel functionalization strategy based on C(sp^3)–C(sp^2) Suzuki–Miyaura cross-coupling reactions of an oxetane-substituted primary alkyl-trifluoroborate **3** and halogenated diphenylamine intermediates (DPA). By the permutation of oxetane-substituted and unsubstituted DPA compounds and central MIF components in the last stage of the synthesis, a set of eight materials was obtained. The set allows for a systematic investigation of the influence of structural parameters on process-relevant parameters for the fabrication of multilayer OLEDs from solution.

Two of the new materials (0L-2G6 **9d** and 4L6-2G6 **9h**) have been used as HTM in standardized OLED architectures. The sixfold-functionalized compound 4L6-2G6 **9h** yielded only moderate device efficiencies, probably due to unreacted oxetane units within the layer. On the other hand, the performance of an OLED containing the twofold-functionalized 0L-2G6 **9d** surpassed the previously used reference materials QUPD and OTPD, underlining the potential of dihydroindenofluorene compounds for hole transport.

Experimental Section

Details of experimental conditions, instrumental methods, molecular structures of reference compounds, OLED fabrication and characterization, NMR spectra and structures for signal assignment, thermogravimetric analyses, and crystallographic data of compounds **6** (CCDC 1913627) and **9a** (CCDC 1913636) can be found in the Supporting Information.

Acknowledgements

The authors would like to thank Christian Rüttiger (Rehahn group, Technical University of Darmstadt) for conducting the DSC measurements, Maurice Heid (Vogel group, Technical University of Darmstadt) for thermogravimetric analysis and the Plenio group (Technical University of Darmstadt) for instrumental support. We gratefully acknowledge financial support by the German Federal Ministry of Education and Research (BMBF, POESIE project). Open access funding enabled and organized by Projekt DEAL.

Conflict of Interest

The authors declare no conflict of interest.

Keywords: crosslinking · materials science · OLEDs · oxetanes · polymerization

[1] P. Kumar, K. N. Shivananda, W. Zajączkowski, W. Pisula, Y. Eichen, N. Tessler, *Adv. Funct. Mater.* **2014**, *24*, 2530–2536.
[2] a) T. P. I. Saragi, T. Spehr, A. Siebert, T. Fuhrmann-Lieker, J. Salbeck, *Chem. Rev.* **2007**, *107*, 1011–1065; b) D. Kolosov, D. S. English, V. Bulovic, P. F. Barbara, S. R. Forrest, M. E. Thompson, *J. Appl. Phys.* **2001**, *90*, 3242–3247; c) L. Ke, P. Chen, S. J. Chua, *Appl. Phys. Lett.* **2002**, *80*, 697–699; d) J. McElvain, H. Antoniadis, M. R. Hueschen, J. N. Miller, D. M. Roitman, J. R. Sheats, R. L. Moon, *J. Appl. Phys.* **1996**, *80*, 6002–6007.
[3] a) K. Naito, A. Miura, *J. Phys. Chem.* **1993**, *97*, 6240–6248; b) K. Naito, *Chem. Mater.* **1994**, *6*, 2343–2350.
[4] T. Saegusa, *J. Macromol. Sci. A.* **1972**, *6*, 997–1026.
[5] a) M. S. Bayerl, T. Braig, O. Nuyken, D. C. Müller, M. Groß, K. Meerholz, *Macromol. Rapid Commun.* **1999**, *20*, 224–228; b) S. Jungermann, N. Riegel, D. Müller, K. Meerholz, O. Nuyken, *Macromolecules* **2006**, *39*, 8911–8919; c) P. Zacharias, M. C. Gather, M. Rojahn, O. Nuyken, K. Meerholz, *Angew. Chem. Int. Ed.* **2007**, *46*, 4388–4392; *Angew. Chem.* **2007**, *119*, 4467–4471; d) G. Liaptsis, K. Meerholz, *Adv. Funct. Mater.* **2013**, *23*, 359–365.
[6] a) C. D. Muller, A. Falcou, N. Reckefuss, M. Rojahn, V. Wiederhirn, P. Rudati, H. Frohne, O. Nuyken, H. Becker, K. Meerholz, *Nature* **2003**, *421*, 829–833; b) G. Liaptsis, D. Hertel, K. Meerholz, *Angew. Chem. Int. Ed.* **2013**, *52*, 9563–9567; *Angew. Chem.* **2013**, *125*, 9742–9746; c) C. Ulbricht, N. Rehmann, E. Holder, D. Hertel, K. Meerholz, U. S. Schubert, *Macromol. Chem. Phys.* **2009**, *210*, 531–541.
[7] O. Nuyken, R. Böhner, C. Erdmann, *Macromol. Symp.* **1996**, *107*, 125–138.
[8] J. Barche, S. Janietz, M. Ahles, R. Schmechel, H. von Seggern, *Chem. Mater.* **2004**, *16*, 4286–4291.

[9] J. Salbeck, N. Yu, J. Bauer, F. Weissörtel, H. Bestgen, *Synth. Met.* **1997**, *91*, 209–215.
[10] a) J. Jacob, J. Zhang, A. C. Grimsdale, K. Müllen, M. Gaal, E. J. W. List, *Macromolecules* **2003**, *36*, 8240–8245; b) D. Vak, B. Lim, S.-H. Lee, D.-Y. Kim, *Org. Lett.* **2005**, *7*, 4229–4232; c) D. Horhant, J.-J. Liang, M. Virboul, C. Poriel, G. Alcaraz, J. Rault-Berthelot, *Org. Lett.* **2006**, *8*, 257–260; d) C. Poriel, J.-J. Liang, J. Rault-Berthelot, F. Barrière, N. Cocherel, A. M. Z. Slawin, D. Horhant, M. Virboul, G. Alcaraz, N. Audebrand, L. Vignau, N. Huby, G. Wantz, L. Hirsch, *Chem. Eur. J.* **2007**, *13*, 10055–10069.
[11] a) S.-Y. Ku, L.-C. Chi, W.-Y. Hung, S.-W. Yang, T.-C. Tsai, K.-T. Wong, Y.-H. Chen, C.-I. Wu, *J. Mater. Chem.* **2009**, *19*, 773–780; b) W. Zhang, J. Smith, R. Hamilton, M. Heeney, J. Kirkpatrick, K. Song, S. E. Watkins, T. Anthopoulos, I. McCulloch, *J. Am. Chem. Soc.* **2009**, *131*, 10814–10815; c) Z. Zhong, X. Wang, T. Guo, J. Cui, L. Ying, J. Peng, Y. Cao, *Org. Electron.* **2018**, *53*, 35–42; d) C. Duan, W. Cai, C. Zhong, Y. Li, X. Wang, F. Huang, Y. Cao, *J. Polym. Sci. Part A* **2011**, *49*, 4406–4415.
[12] a) H. Kim, N. Schulte, G. Zhou, K. Müllen, F. Laquai, *Adv. Mater.* **2011**, *23*, 894–897; b) F. Eckes, A. Gerhard, A. Hayer, H. Heil, D. Joosten (WO 2013/156125 A1), **2013**.
[13] M. Hempe, M. Reggelin, *RSC Adv.* **2017**, *7*, 47183–47189.
[14] S. D. Dreher, S.-E. Lim, D. L. Sandrock, G. A. Molander, *J. Org. Chem.* **2009**, *74*, 3626–3631.
[15] E. Bacher, S. Jungermann, M. Rojahn, V. Wiederhirn, O. Nuyken, *Macromol. Rapid Commun.* **2004**, *25*, 1191–1196.
[16] a) S. Setayesh, D. Marsitzky, K. Müllen, *Macromolecules* **2000**, *33*, 2016–2020; b) K.-T. Wong, L.-C. Chi, S.-C. Huang, Y.-L. Liao, Y.-H. Liu, Y. Wang, *Org. Lett.* **2006**, *8*, 5029–5032.
[17] H. S. M. Kodomari, S. Yoshitomi, *J. Org. Chem.* **1988**, *53*, 2093.
[18] H. H. Fan, L. Guo, K. F. Li, M. S. Wong, K. W. Cheah, *J. Am. Chem. Soc.* **2012**, *134*, 7297–7300.
[19] J. V. Crivello, J. L. Lee, *J. Polym. Sci. Part A* **1989**, *27*, 3951–3968.
[20] J. K. Gillham, *Polym. Eng. Sci.* **1986**, *26*, 1429–1433.
[21] S. Feser, K. Meerholz, *Chem. Mater.* **2011**, *23*, 5001–5005.

Manuscript received: August 29, 2019
Revised manuscript received: October 2, 2019
Accepted manuscript online: October 22, 2019

Addition: Correction added on 20. November 2020, after first online publication: Projekt Deal funding statement has been added.